VBIC95: An Improved Vertical, IC Bipolar Transistor Model

Colin McAndrew	AT&T/Motorola	2100 E. Elliot Rd., Tempe, AZ 85284
Jerry Seitchik	Texas Instruments	P.O. Box 655012, Dallas, TX 75265
Derek Bowers	Analog Devices	1502 Harrison Crt., Sunnyvale, CA 94087
Mark Dunn	Hewlett-Packard	1400 Fountaingrove Pkwy., Santa Rosa, CA 95043
Mark Foisy	Motorola	3501 Ed Bluestein Blvd., Austin, TX 78721
Ian Getreu	Analogy	9205 S.W. Gemini Dr., Beaverton, OR 97075
Marc McSwain	MetaSoftware	1300 White Oaks Rd., Campbell, CA 95008
Shahriar Moinian	AT&T Bell Laboratories	2525 N. 12th St., Reading, PA 19612.
James Parker	National Semiconductor	2900 Semiconductor Dr., Santa Clara, CA 95052
Paul van Wijnen	Intel/Philips	2200 Mission College Blvd., Santa Clara, CA 95052
Larry Wagner	IBM	1580 Rt. 52, Hopewell Junction, NY 12533

ABSTRACT

This paper presents a vertical BJT model developed by IC and CAD industry representatives as a replacement for the SPICE Gummel-Poon model. VBIC95 includes improved modeling of the Early effect (output conductance), substrate current, quasi-saturation, and behavior over temperature.

I. INTRODUCTION

The SPICE Gummel-Poon (SGP) model [1,2] has remained essentially unchanged for over 20 years. While this is a testimony to its elegant, intuitive, and physically consistent formulation, it has been long known that the SGP model has short-comings. Improved models have been published [3-7]; however, none has supplanted the SPICE 2G6 GP model as the *de facto* standard. To rectify this situation, a group of representatives from the IC and CAD industries collaborated to recommend an improved standard BJT model for the semiconductor industry.

The initial charter of the group was to evaluate BJT models developed since the SGP model, recommend the best model, and work to bring it into the mainstream of IC design. However the models evaluated did not satisfy all requirements of the committee, so action was taken to formulate a model that did. The major requirements were as follows. First, the model should overcome the major deficiencies of the SGP model. Second, complete source code, documentation, and extraction algorithms should be publicly available. Third, with default parameters the model should simplify to be as similar as possible to the SGP model. Fourth, the model should be C_∞-continuous.

In this paper we will review the basics of BJT modeling, and the deficiencies of the SGP model for modern BJTs. We will then give details of the VBIC95 (Vertical Bipolar Inter-Company, 1995) model, and the reasons that underlie choices made during its formulation.

Our framework is a vertical NPN IC transistor, fabricated in a P-type substrate. We thus consider only a 4-terminal vertical model and work in NPN polarities. Many of the features also make the model suitable for other structures and PNP transistors. We will signify base, emitter, collector and substrate by the letters b, e, c, and s, respectively, and currents flowing into these terminals as I_b, I_e, I_c, and I_s.

II. REVIEW OF BJT DEVICE PHYSICS

In this section we will review 1-dimensional analyses of I_c and I_b. The analysis of Gummel and Poon [1] is still today the best description of bipolar behavior, and is the basis for VBIC95. The review here follows [8,9].

We start with the electron continuity equation

$$q(\partial n/\partial t)-\nabla\cdot\mathbf{J}_e = q(G_e-R_e) \quad (1)$$

and the drift-diffusion relation

$$\mathbf{J}_e = -q\mu_e n\nabla\psi+qD_e\nabla n = -q\mu_e n\nabla\phi_e, \quad (2)$$

where the symbols have their usual meaning. In steady state and 1-dimension, ignoring recombination and generation, $\partial J_{ex}/\partial t=0$ so we have

$$J_{ex} = q\mu_e n_{ie}V_{tv}\exp(\psi/V_{tv})\partial\exp(-\phi_e/V_{tv})/\partial x = \text{constant}. \quad (3)$$

Here $V_{tv}=kT/q$ is the thermal voltage, and the mobile carrier densities n and p are related to the electron and hole quasi-Fermi levels ϕ_e and ϕ_h and the effective intrinsic concentration n_{ie} (including bandgap narrowing) via

$$n = n_{ie}\exp((\psi-\phi_e)/V_{tv}),\ p = n_{ie}\exp((\phi_h-\psi)/V_{tv}) \quad (4)$$

where ψ is the electrostatic potential.

Integrating Eq. (2) from x=0 at the emitter to x=w at the collector, through the base, gives

$$J_{ex} = (qV_{tv}(\exp(-\phi_{ew}/V_{tv})-\exp(-\phi_{e0}/V_{tv}))) \Big/ \int_o^w (\exp(-\psi(x)/V_{tv})/(\mu_e(x)n_{ie}(x))\,dx \quad (5)$$

where the explicit dependencies of ψ, μ_e and n_{ie} on x are noted. Now ϕ_h is nearly constant across the base region of a BJT (in fact it is convenient to define the base as the portion of an NPN BJT where ϕ_h is close to constant, as this consistently includes the case of base pushout) and the junction voltages of the intrinsic device are related to the quasi-Fermi levels by

$$V_{bei} = \phi_h-\phi_{e0},\ V_{bci} = \phi_h-\phi_{ew}. \quad (6)$$

Therefore, multiplying both the numerator and the denominator of the right side of Eq. (5) by $\exp(\phi_h/V_{tv})$, multiplying by the emitter area A_e to convert current density to current, noting that the transport current I_{cc} is defined as positive when flowing in the negative x direction, and using Eq. (4), gives the fundamental Gummel-Poon relation

0-7803-2778-0/95/$4.00

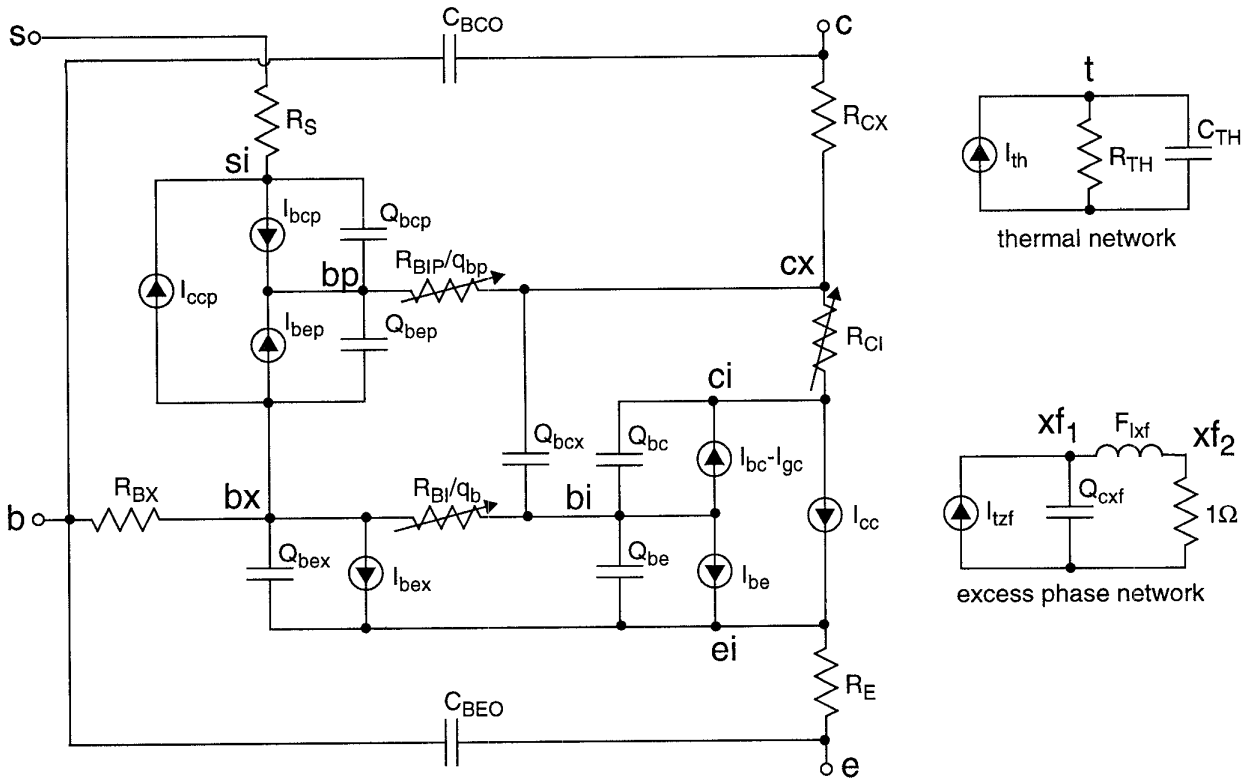

Figure 1. Equivalent Network for VBIC95

$$I_{cc} = I_S(\exp(V_{bei}/V_{tv})-\exp(V_{bci}/V_{tv}))/q_b. \quad (7)$$

The saturation current I_S is

$$I_S = qA_eV_{tv}/G_{b0} \quad (8)$$

and the normalized base charge q_b is

$$q_b = G_b/G_{b0}. \quad (9)$$

The base charge, weighted by mobility and the square of the effective intrinsic carrier concentration, is

$$G_b = \int_o^w p/(\mu_e(x)n_{ie}^2(x))\,dx \quad (10)$$

and G_{b0} is the value of G_b at equilibrium.

The Gummel-Poon integral charge control relationship (ICCR) leads to Eq. (7) for the transport current in a BJT. The modeling of q_b, addressed below, includes depletion charge components, which give rise to the Early effect, and the significant increase of the base charge with bias under high level injection, the Webster effect.

The base current supplies holes that recombine in the b-e space-charge region (the depletion region around the b-e junction), in the quasi-neutral emitter, and at the emitter contact. The net recombination rates for the Shockley-Read-Hall and Auger process are

$$R_{srh} = (np-n_{ie}^2)/(\tau_h(n+n_{ie})+\tau_e(p+n_{ie})), \quad (11)$$

$$R_{aug} = (c_en+c_hp)(np-n_{ie}^2). \quad (12)$$

The base current due to recombination in the b-e space-charge region is dominated by R_{srh}, because although we have $pn \gg n_{ie}^2$ both n and p are relatively small, so R_{aug} is small. Through the space-charge region, $\phi_e \approx 0$ and $\phi_h \approx V_{bei}$, so from Eqs. (4) and (11)

$$R_{sc,srh} \approx n_{ie}\exp(V_{bei}/V_{tv}) / \quad (13)$$
$$(\tau_h(\exp(\psi/V_{tv})+1)+\tau_e(\exp((V_{bei}-\psi)/V_{tv})+1))$$

from which it follows that the maximum $R_{sc,srh}$ occurs for

$$\psi = 0.5(V_{bei}-V_{tv}\log_e(\tau_h/\tau_e)) \quad (14)$$

and, for $\tau_h \approx \tau_e$, has a value

$$R_{sc,srh}(max) = n_{ie}\exp(V_{bei}/V_{tv}) / \quad (15)$$
$$((\tau_h+\tau_e)(\exp(0.5V_{bei}/V_{tv})+1)).$$

Thus the space-charge region component of I_b, the integral of $R_{sc,srh}$, is nearly proportional to $\exp(0.5V_{bei}/V_{tv})$.

For the quasi-neutral component, $n \approx N_d$ (the emitter doping), $\phi_e \approx 0$ and so from Eq. (4)

$$p \approx n_{ie}^2\exp(\phi_h/V_{tv})/N_d \ll n. \quad (16)$$

It follows that $np \gg n_{ie}^2$ and so

$$R_{qn,srh} \approx p/\tau_h = n_{ie}^2\exp(\phi_h/V_{tv})/(N_d\tau_h) \quad (17)$$

$$R_{qn,aug} \approx c_en^2p = c_eN_dn_{ie}^2\exp(\phi_h/V_{tv}) \quad (18)$$

and thus the quasi-neutral region recombination component of I_b, the integral of $R_{qn,srh}$ and $R_{qn,aug}$, is proportional to $\exp(V_{bei}/V_{tv})$, because $\phi_h \approx V_{bei}$ where this recombination is largest.

The hole surface recombination velocity S_h at the emitter determines the hole recombination rate there. The recombination current density at the emitter contact is

$$J_{h,ec} = qS_h(p_{ec}-p_{ec0}) \quad (19)$$

where p_{ec0} is the equilibrium hole concentration at the emitter contact. For a shallow emitter with negligible recombination in the quasi-neutral region,

$$p_{ec} \approx n_{ie}^2 \exp(V_{bei}/V_{tv})/(N_d(1+S_h w_e/D_h)) \quad (20)$$

where w_e is the emitter depth, so like the quasi-neutral component, the emitter contact component of I_b is proportional to $\exp(V_{bei}/V_{tv})$.

III. DEFICIENCIES IN THE SGP MODEL

Unlike MOSFET models, which have proliferated greatly (there are over 50 different MOSFET models in the widely used HSPICE simulator), the SGP model is still the most widely used BJT model today, 20 years after its introduction. However, it has become too inaccurate for low risk design in modern technologies.

A major reason for the decrease in accuracy of the SGP model has been the changes in BJT device technology over the past decades. Reduced base widths mean that the approximations made in the Early effect model in [2] give unacceptably large errors in modeling output conductance, g_o, in modern devices. Also, shrinking device dimensions and changes in device structures mean that parasitic capacitances not accounted for in the SGP model are now important, e.g. the parasitic b-e capacitance from the dielectric between base and emitter metallization. Changes in doping profiles mean that collector resistance R_{CI} modulation (e.g. base push-out) is important. Although this was recognized in the early 1960's it has only recently begun to percolate into the mainstream of simulation and design. Base push-out affects AC modeling as well.

Parasitic substrate transistor action is important for modeling, but is not included in the SGP model. Accurate substrate current modeling is required both for designs in which the substrate transistor can turn on and for designs where it is meant not to turn on. For the latter, accurate modeling of the turning on of the substrate transistor serves to warn designers about design problems.

Other deficiencies of the SGP model include: poor scaling with geometry (although more accurate scaling can be done by using different models for different geometries, it is still desirable to have a model that scales with geometry, as diode, resistor and MOSFET models do); inadequate modeling of high-frequency effects; inadequate modeling of temperature effects; lack of modeling of avalanche effects; and no modeling of self-heating.

IV. VBIC95 MODEL OVERVIEW

Fig. 1 shows the equivalent circuit for the VBIC95 model. Compared with the SGP model, VBIC95 includes the following features that make it topologically distinct from the SGP model. The parasitic substrate PNP is modeled by a simplified GP transistor, quasi-saturation is modeled after [4] with the elements R_{CI}, Q_{bcx}, and a modified Q_{bc}, and by including the elements I_{bex} and Q_{bex}, along with R_{BI}, I_{be} and Q_{be}, the distributed nature of the base is modeled to a first order. Excess phase is modeled with a second-order network that implements the Weil-McNamee approximation [10]. A weak avalanche current I_{gc} is included for the b-c junction. Finally, to model capacitances associated with extrinsic parasitics, the constant capacitances C_{BEO} and C_{BCO} are included. Note that in Fig. 1 the intrinsic base resistances, R_{BI} and R_{BIP}, are modulated by the normalized base charges, q_b and q_{bp}, respectively, and the intrinsic collector resistance, R_{CI}, is modulated by V_{bci}. Therefore, they are really current sources that depend on more than one controlling voltage, but they are drawn as resistors for easier understanding.

A self-heating model will be released as a separate option for VBIC95. The model includes the thermal resistance R_{TH} and capacitance C_{TH}, along with the thermal power source I_{th}, which couples the power generated in the BJT to the thermal network. The local temperature rise at node t is linked to the electrical model through the temperature mappings of the model parameters.

The default parameters for VBIC95 are such that the elements of the model that are topologically distinct from the SGP model are turned off. However, this does not make VBIC95 default to SGP under these circumstances. The Early effect approximation in the SGP model is known to cause inaccuracies in output conductance modeling for modern BJTs [11], so an Early effect model based on the junction depletion charges is used in VBIC95. As Fig. 2 shows, this both qualitatively and quantitatively improves output conductance modeling. However, this means that existing SGP model parameter sets need to have the Early voltages adjusted to work reasonably with VBIC95.

One final axiom underlies VBIC95. Many compact models of semiconductor devices are conditional, in that they use different equations to model behavior in different regions of operation. This is more common in MOSFET models, where separation into subthreshold, triode, and saturation region operation is common, but is also found in the junction capacitance and current portions of the SGP model. Real semiconductor devices do not, in general, exhibit distinct regions of operation, but make smooth transitions between regions where different approximations to detailed transport models become more accurate than others. Therefore, regional models can be inaccurate near boundaries between regions and can cause problems for many numerical methods used for circuit simulation, can limit the applicability of advanced numerical algorithms for circuit simulation, and can limit the accuracy of distortion analyses. VBIC95 is based on single-piece, smooth functions. There are two exceptions to this. First, conditional statements are allowed to avoid numerical catastrophes, such as divide by zero. Second, while a smooth depletion charge/capacitance model is available in VBIC95, for backward compatibility the SGP depletion charge/capacitance model, which is a regional model, is also included (and is the default).

VBIC95 includes noise models similar to those of the SGP model, with shot, thermal, and 1/f components.

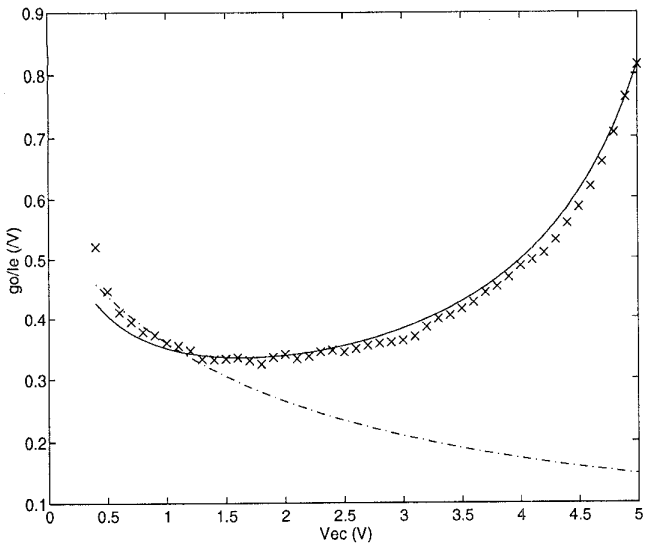

Figure 2. Output Conductance (Reverse Region, Detail)
xxxx data –·– SGP ——VBIC95

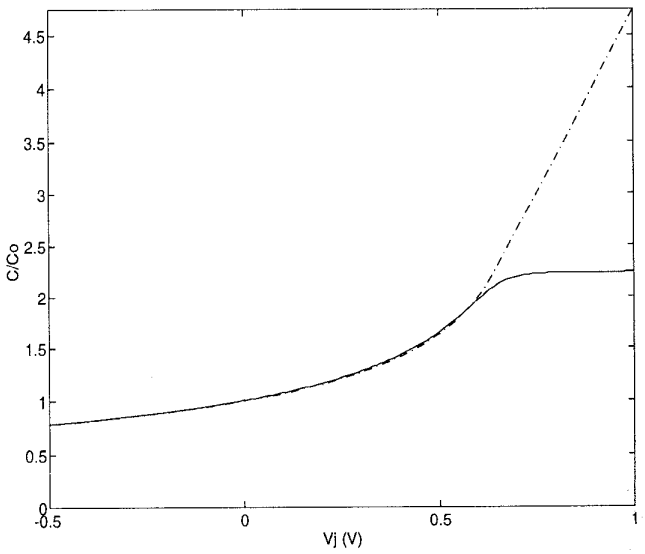

Figure 3. Depletion Capacitance Models
–·– piecewise (SGP) ——smooth, single-piece

V. BRANCH CONSTITUTIVE RELATIONS

Below the branch voltages used are: $V_{bei}=V_{bi}-V_{ei}$, $V_{bci}=V_{bi}-V_{ci}$, $V_{bcx}=V_{bi}-V_{cx}$, $V_{bep}=V_{bx}-V_{bp}$, $V_{bcp}=V_{si}-V_{bp}$, $V_{beo}=V_b-V_e$, and $V_{bco}=V_b-V_c$, where V_{bi} is the voltage on node bi in Fig. 1, and so on.

The forward transport current is, from above, [1]

$$I_{cc} = (I_{tf} - I_{tr})/q_b \tag{21}$$

$$I_{tf} = I_S(\exp(qV_{bei}/N_FkT)-1),\ I_{tr} = I_S(\exp(qV_{bci}/N_RkT)-1)$$

where I_{tf} and I_{tr} are the forward and reverse transport currents. Separate nonideality factors N_F and N_R are included for forward and reverse components of I_{cc}, for compatibility with the SGP model. However, we recommend using $N_F=N_R$ otherwise under certain circumstances the model can become non-passive (i.e. can generate power).

The model Eq. (21) derives from the analysis given above, and is the same form as the SGP model of [2]; however q_b is modeled differently. Rather than using the approximation of [2], we use the proper formulation [1,11]

$$q_b = q_1+q_2/q_b \tag{22}$$

$$q_1 = 1+q_{je}/V_{ER}+q_{jc}/V_{EF},\ q_2 = I_{tf}/I_{KF}+I_{tr}/I_{KR}$$

where the b-e and b-c depletion charges are

$$q_{je} = q_j(V_{bei},P_E,M_E),\ q_{jc} = q_j(V_{bci},P_C,M_C). \tag{23}$$

Here V_{EF} and V_{ER} are forward and reverse Early voltages, I_{KF} and I_{KR} are forward and reverse knee currents, and P_E, P_C and M_E, M_C are the built-in potentials and grading coefficients of the b-e and b-c junctions. q_1 is smoothly limited to be greater than 0.0001, to avoid numerical problems.

VBIC95 has two models for the depletion charge function q_j. The first is the standard piecewise model of SPICE 2G6, e.g. [2]. The second is a single-piece model, similar to [12], for which the capacitance smoothly limits to a constant value for junction biases greater than the built-in potential (see Fig. 3). This gives a good transition between the bias regimes where depletion and diffusion effects dominate the junction capacitance.

From the above, the basis of the ICCR is the depletion and diffusion charges in the base. Consistency of the I_{cc} and charge models implies that

$$C_{JE}V_{ER} = C_{JC}V_{EF}(A_e/A_c) = \tau_F I_{KF} = \tau_R I_{KR} \approx Q_{b0} \tag{24}$$

should hold, where A_c is the area of the collector, C_{JC} is scaled by A_e/A_c for consistency with the 1-dimensional analysis above, and $Q_{b0}=A_e\int_o^w p\,dx$. C_{JE} and C_{JC} are the zero bias b-e and b-c junction capacitances, τ_F and τ_R the forward and reverse transit times, and these are used in charge modeling in place of the Early voltages and knee currents. As with the original SGP model, the above relationships are not enforced in VBIC95. This is for backward compatibility and also because it recognizes that the model involves approximations, so introducing separate parameters for DC and AC modeling allows more flexibility in modeling and simplifies parameter extraction.

If the excess phase model of VBIC95 is used, I_{tf} above is modified as follows. I_{tzf} in Fig. 1 is driven by I_{tf} from above. If the capacitance of the charge element Q_{cxf} is C and the inductance of the flux element F_{lxf} is L, then the voltage at node xf_2 is

$$V_{xf2} = (1/LC)/(s^2+s/L+1/LC) \tag{25}$$

which, on setting $L=T_D/3$ and $C=T_D$, where $T_D=1/\omega_0$ is a parameter of VBIC95, is just the second-order Bessel polynomial approximation to excess phase of [10]. V_{xf2} is then used to drive I_{cc}. Note that this implementation is consistent between AC and transient analyses and is independent of the numerical algorithm used for integration.

The transport current I_{ccp} of the parasitic PNP transistor is modeled similarly to I_{cc}, with the following differences. First, because the parasitic is distributed between intrinsic (under the emitter) and extrinsic (not under the emitter)

components, the control of the forward component of I_{ccp} is split between V_{bep} and V_{bci} as follows,

$$I_{tfp} = I_{SP}(W_{SP}\exp(qV_{bep}/N_{FP}kT)+ \quad (26)$$
$$(1-W_{SP})\exp(qV_{bci}/N_{FP}kT)-1).$$

Second, no Early effect is included, and high level injection is modeled only for the forward component, so

$$q_{bp} = 1+q_{2p}/q_{bp},\ q_{2p} = I_{tfp}/I_{KP} \quad (27)$$

is the normalized base charge for the parasitic PNP.

The physical analysis of section II shows that I_b is associated with a different physical mechanism than I_c, therefore rather than linking I_b and I_c by a phenomenological $\beta_F=I_c/I_b$ (in forward mode operation), the b-e and b-c components of base current are modeled independently of I_c. The total b-e component of base current is

$$I_{bt} = I_{BEI}(\exp(V_{bei}/(N_{EI}V_{tv}))-1) \quad (28)$$
$$+I_{BEN}(\exp(V_{bei}/(N_{EN}V_{tv}))-1)$$

and this is apportioned between intrinsic and extrinsic parts

$$I_{be} = W_{BE}I_{bt},\ I_{bex} = (1-W_{BE})I_{bt}. \quad (29)$$

The apportioning is done for two reasons. First, it is a first order approximation to modeling the distributed nature of the base, for both DC and AC modeling. Second, when switching from large reverse bias on V_{be} and V_{bc}, the base is depleted of mobile carriers and R_{BI}/q_b becomes large. This causes erroneous simulation results because the device is predicted to support a large forward V_{be} until the base charges up. In reality the transistor turns on at the edges of the base first and does not support the large forward V_{be}. This is a deficiency of the 1-dimensional analysis, which does not account for this 2-dimensional phenomenon. The apportioning of the b-e component of base current into I_{be} and I_{bex} overcomes this problem.

The ideal component of I_{bt}, associated with the saturation current I_{BEI} and the emission coefficient N_{EI}, corresponds to recombination in the quasi-neutral emitter and at the emitter contact, so N_{EI} is close to 1. The nonideal component, modeled with I_{BEN} and N_{EN}, corresponds to recombination in the b-e space-charge region, N_{EN} is of order 2.

The b-c component of base current is

$$I_{bc} = I_{BCI}(\exp(V_{bci}/(N_{CI}V_{tv}))-1)+ \quad (30)$$
$$I_{BCN}(\exp(V_{bci}/(N_{CN}V_{tv}))-1)$$

and a similar model, including ideal and nonideal components, is used for I_{bep} and I_{bcp}. I_{bc} is augmented by a weak avalanche current, $-I_{gc}$, modeled as in [13]

$$I_{gc} = (I_{cc}-I_{bc})A_{VC1}(P_C-V_{bci})\exp(-A_{VC2}(P_C-V_{bci})^{ME-1}) \quad (31)$$

where A_{VC1} and A_{VC2} are model parameters.

The resistances R_{BX}, R_E, R_{CX}, and R_S are modeled as constants. The intrinsic base resistance R_{BI} is modulated by q_b, as noted in [1]. The SGP model includes two choices for modeling the bias dependence of R_{BI}. One is q_b modulation as in VBIC95. The other models the distributed base

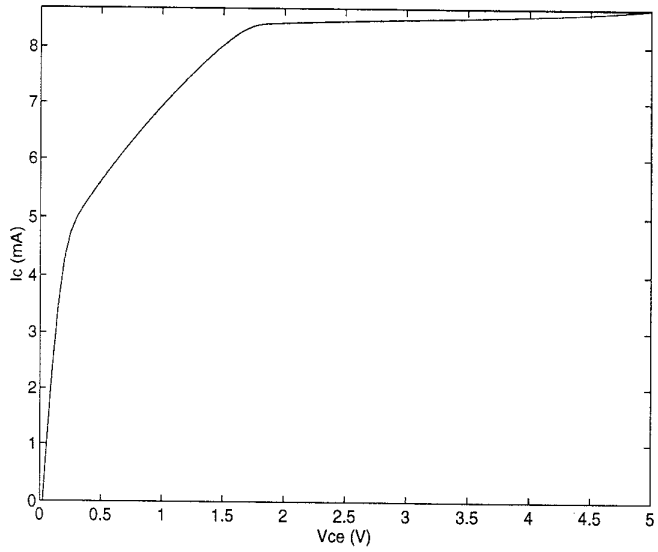

(a) collector current

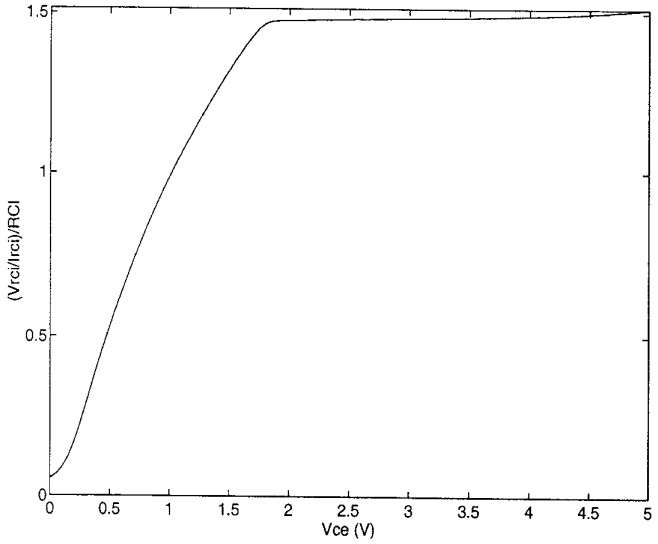

(b) normalized epi resistance

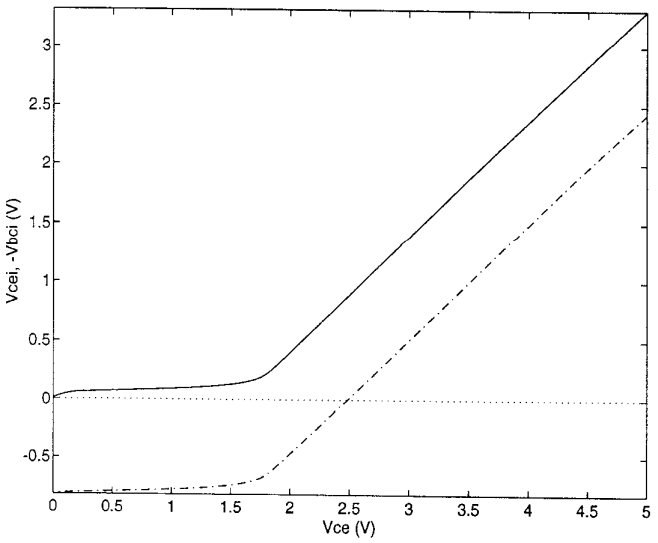

(c) internal device biases —— V_{cei} -·-· $-V_{bci}$

Figure 4. Quasi-sat Model Characteristics

effect that causes DC emitter crowding. In VBIC95, emitter crowding, both DC and AC, is modeled to a first order by the splitting of the b-e current and charge across R_{BI}. The intrinsic base resistance of the parasitic R_{BIP} is modulated by the normalized parasitic base charge q_{bp}.

The modeling of the current in the intrinsic collector (epi) region is based on the analysis of [4]. Although the model of [4] has been adopted in the major commercial SPICE simulators, it is only recently becoming widely known that the model of [4] can predict negative g_o at high V_{be}. If the velocity saturation model in [4] is ignored, then the current in the epi is

$$I_{epi0} = \left(V_{rci} + V_{tv}\left(K_{bci} - K_{bcx} - \log_e\left((K_{bci}+1)/(K_{bcx}+1)\right)\right)\right)/R_{CI} \quad (32)$$

$$K_{bci} = (1+\gamma\exp(V_{bci}/V_{tv}))^{1/2},\ K_{bcx} = (1+\gamma\exp(V_{bcx}/V_{tv}))^{1/2}$$

where $V_{rci} = V_{bci} - V_{bcx}$. In [4] this is coupled with a velocity saturation model $\mu = \mu_0/(1+\mu_0|\nabla\phi_e|/v_{sat})$ where v_{sat} is the electron saturation speed. This modifies the denominator above to become $R_{CI}(1+|V_{rci}|/V_O)$ where $V_O = w_{epi}v_{sat}/\mu_0$. This velocity saturation model is undesirable because it introduces discontinuities in high order derivatives and because it causes the negative g_o. By using the alternative model $\mu = \mu_0/(1+(\mu_0\nabla\phi_e/v_{sat})^2)^{1/2}$, and by using $I_{epi0}R_{CI}$ in stead of V_{rci} in this model, both of the problems are overcome. Further, we empirically change V_O with V_{rci}, through the high R_C parameter H_{RCF}, to account for the increase in collector current with increased V_{rci} at high V_{bci}. The final model for the current in R_{CI} is

$$I_{rci} = I_{epi0}/\left(1+\left(I_{epi0}R_{CI}/\left(V_O\left(1+0.5\left(V_{rci}^2+0.01\right)^{1/2}/(V_O H_{RCF})\right)\right)\right)^2\right)^{1/2} \quad (33)$$

where a smooth approximation to $|V_{rci}|$ has been used to avoid numerical problems and preserve high order continuity. Fig. 4 shows I_c from the quasi-sat model, along with $(V_{rci}/I_{rci})/R_{CI}$, which shows how the intrinsic collector resistance is modulated with bias, and the internal voltages V_{cei} and V_{bci}, which clearly show the onset of internal saturation. Note that at high V_{ce} the epi resistance exceeds R_{CI}, because of velocity saturation.

A self-heating model is defined for VBIC95. The thermal power I_{th} is the sum of the products of the currents through and voltages across each non-storage element of the electrical network. R_{TH} and C_{TH} are the (linear) thermal resistance and capacitance of the BJT.

Depletion capacitances, from the model described above, are used for the b-e junction (with C_{JE} partitioned across R_{BI} by W_{BE}, just as for the junction current), for the b-c junction (split into C_{JC} and C_{JEP} for the intrinsic and parasitic devices), and for the c-s junction, with zero bias capacitance C_{JCP}. A diffusion charge, τ_F multiplied by I_{tf}, is also included in Q_{be} (this component is not partitioned), and τ_F changes with bias as in the standard SGP model. Q_{bc} and Q_{bep} include diffusion charges, modeled as τ_R multiplied by I_{tr} and I_{tfp}, respectively. Q_{bc} includes a component $Q_{CO}K_{bci}$, which models part of the charge associated with base pushout [4]. The other part is $Q_{bcx} = Q_{CO}K_{bcx}$. Linear capacitors C_{BEO} and C_{BCO} are used to model the fixed (bias independent) parasitic b-e and b-c capacitances, respectively.

VI. TEMPERATURE MAPPINGS

BJT electrical behavior varies with temperature, and so VBIC95 has temperature mappings defined for its model parameters. The mappings are similar to, but improved on, the temperature mappings for the SGP model.

The resistances have a temperature variation

$$R(T_2) = R(T_1)(T_2/T_1)^{XR} \quad (34)$$

where the temperatures are in Kelvin, and there is a separate X_R parameter for each doping type region. This follows an empirical model of the temperature dependence of mobility [14]. Commonly a second order polynomial model is used for resistor temperature variation. However, the above model is preferred as it is invertible and transitive, $R(T_1)=R(T_1\rightarrow T_2\rightarrow T_1)$ and $R(T_1\rightarrow T_3)=R(T_1\rightarrow T_2\rightarrow T_3)$, which are physically sensible properties, and desirable for model implementation.

The transport saturation current varies as

$$I_S(T_2) = I_S(T_1)(r_T^{XIS}\exp(-E_A(1-r_T)/V_{tv}))^{1/NF} \quad (35)$$

where $r_T = T_2/T_1$ and X_{IS} and E_A are parameters. This is similar to the SGP model and is based on the variation of n_{ie}^2 with temperature. The other saturation currents have similar temperature mappings, with separate activation energies for ideal and nonideal components. This allows fitting of β_F and β_R over bias and temperature.

The junction built-in potentials P vary with temperature as $(kT/q)\log_e(n_{n0}p_{p0}/n_{ie}^2)$, which is similar to the SGP model, but avoids the problem with the SGP model of the potentials becoming negative as temperature increases. The zero bias junction capacitances vary as

$$C(T_2) = C(T_1)(P(T_1)/P(T_2))^M \quad (36)$$

where M is the junction grading coefficient. The parameter γ in the quasi-sat model is proportional to n_{ie}^2 [4], and so varies with temperature as Eq. (35). V_O is modeled similarly to Eq. (34), with parameter X_{VO}, and N_F, N_R, and A_{VC2} are modeled as varying linearly with temperature.

VII. PARAMETER EXTRACTION

Because VBIC95 can, by not using advanced features, be made to be similar to the SGP model, existing extraction techniques can be applied for some VBIC95 parameters. However, to use the advanced features of VBIC95 requires determination of the quasi-sat parameters, the partitioning parameters, and the parasitic parameters.

Because the Early effect model, and hence the DC behavior, depends on the depletion charges, the first step is to extract junction depletion capacitance parameters, using optimization. This is a major difference with respect to parameter extraction for the SGP model, where the Early voltages come from DC data only. Forward bias junction capacitance data should be included, up to where the diffusion capacitance becomes non-negligible, to ensure good extraction of the junction built-in potentials. As a rule of

thumb, data up to 2 to 3 times the zero bias capacitance should be included. Separation of C_{JC} and C_{JEP} for the depletion components of Q_{bep} and Q_{bc}, respectively, is based on layout or extractions from different geometries.

The Early voltages are determined by the method of [11] and knee currents from analysis of forward, reverse, and substrate DC current gains (e.g. the knee current is where this gain drops to half its low-current value). These parameters can be further refined by optimization. The saturation currents, emission coefficients, and temperature parameters for all transport and diode-like currents are estimated from low bias data and then refined using optimization. Fitting the low bias parameters is straightforward.

Resistances can be determined using existing methods. However, there is a degree of indeterminacy in extracting resistances from DC data only. Initial extracted resistances are thus refined by simultaneous optimization of AC and DC data (including high bias data) [15]. Transit time parameters and excess phase are likewise extracted using existing techniques and then refined as part of the simultaneous DC and AC optimization.

Parameter extraction methods for VBIC95 are being finalized and a recommended extraction strategy will be available with the code for the model.

VII. EXAMPLES

Fig. 5 shows forward Gummel and forward output characteristics of VBIC95, for a modern device. The ability to model I_c and I_b over a wide range of biases is apparent.

Fig. 6 compares fits of the SGP and VBIC95 models for forward output data from another modern device. The improved fit through the transition to saturation is clear. Fig. 7 compares g_o fits, from the same data as Fig. 6. The significant improvement in conductance modeling, critical for analog circuits, is apparent. The use of the depletion charges in the Early effect mode, the quasi-sat model, and the avalanche model, all contribute to the improved fit.

VIII. CONCLUSIONS

In this paper we have reviewed BJT device physics and the weaknesses of the SGP model for modern BJTs, and given details of VBIC95, a model developed by a group of industry representatives to provide an improved BJT model to replace the SGP model. The intent is to usher into widespread use an improved BJT model. This is why representatives from a number of semiconductor and CAD companies were involved. The goal is to reduce design risk by improving the accuracy of circuit simulations.

Code for VBIC95 is publicly available and includes a pseudo-code description of the model, routines for model evaluation, test programs to verify implementation, and will include extraction software and a program to map from SGP model parameters to VBIC95 model parameters. We expect the code to be on the web in the near future.

Future improvements to VBIC will include a 3-terminal version, improved geometric scaling, and improved b-e diffusion capacitance modeling.

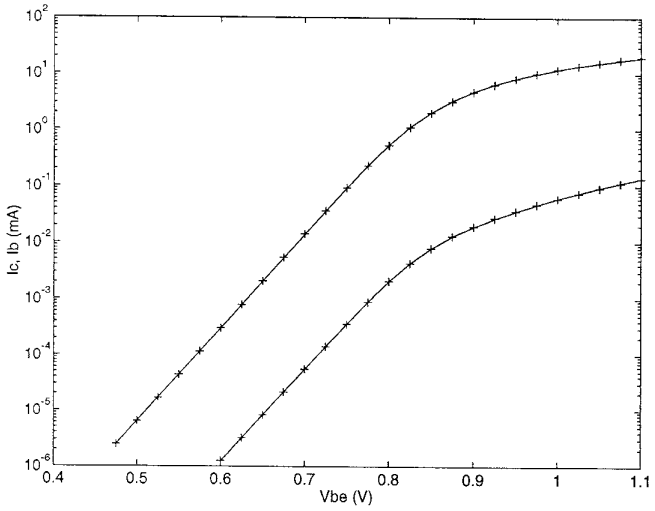

(a) forward Gummel characteristics, I_c top, I_b bottom

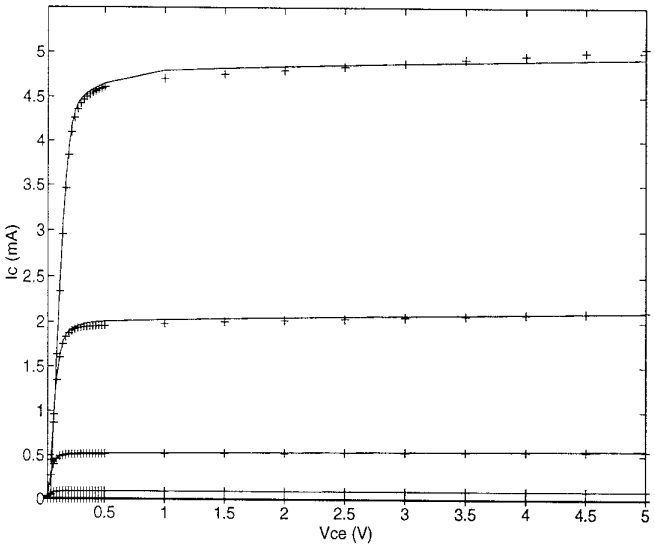

(b) I_c for forward output characteristics

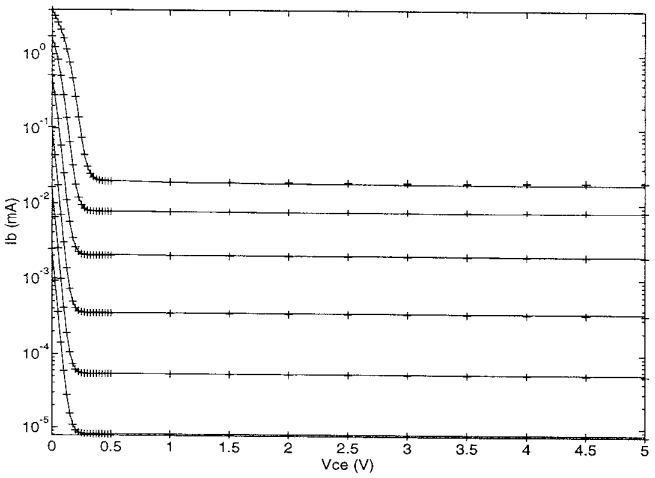

(c) I_b for forward output characteristics

Figure 5. Model Playbacks, ++++data ——VBIC95

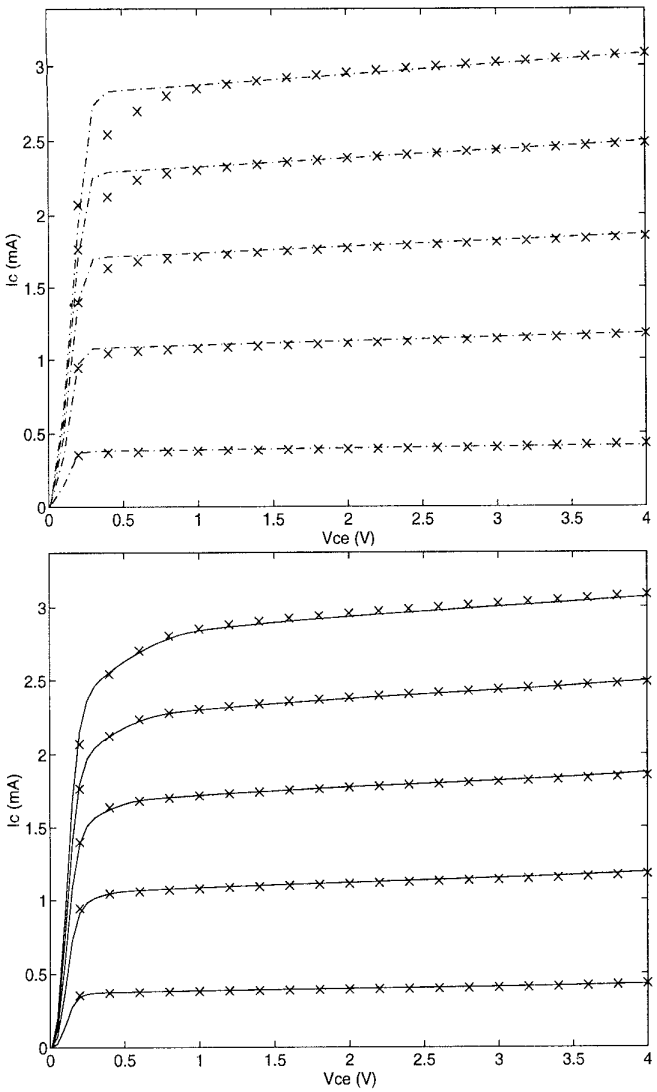

Figure 6. Forward Output I_c Comparison
xxxx data -·-·- SGP ——VBIC95

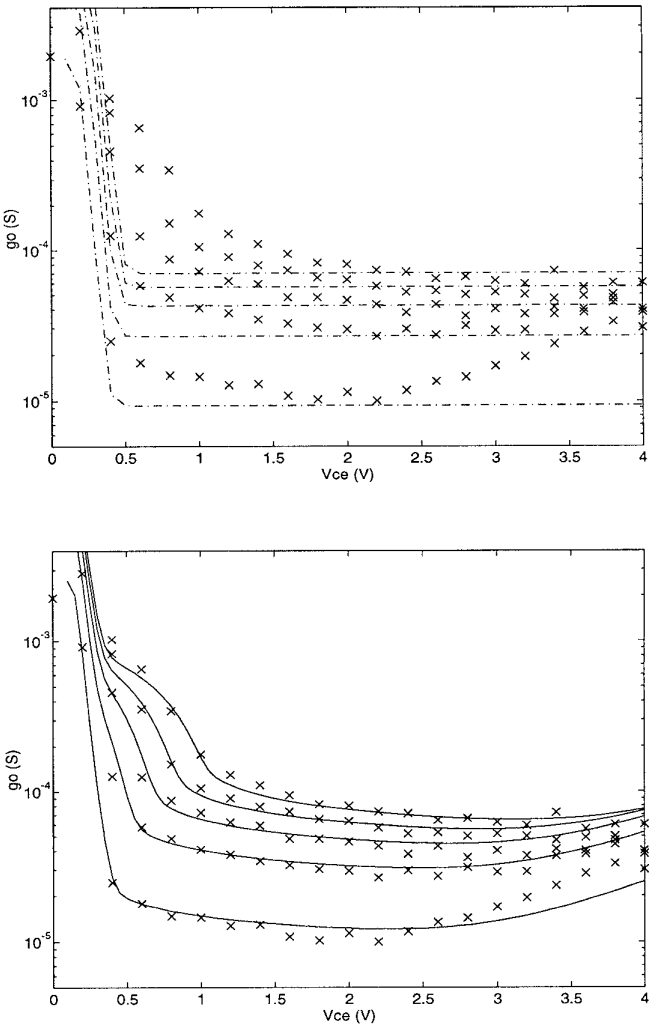

Figure 7. Forward Output g_o Comparison
xxxx data -·-·- SGP ——VBIC95

REFERENCES

[1] H. K. Gummel and H. C. Poon, Bell. System Tech. J., vol. 49, pp. 827-852, May 1970.

[2] L. W. Nagel, Memorandum no. ERL-M520, Electronics Research Laboratory, University of California, Berkeley, May 1975.

[3] L. J. Turgeon and J. R. Mathews, pp. 394-397, Proc. 1980 IEDM.

[4] G. M. Kull, L. W. Nagel, S.-W. Lee, P. Lloyd, E. J. Prendergast, and H. K. Dirks, IEEE Trans. Electron Dev., vol. 32, no. 6, pp. 1103-1113, Jun. 1985.

[5] H. C. de Graaff and W. J. Kloosterman, IEEE Trans. Electron Dev., vol. 32, no. 11, pp. 2415-2419, Nov. 1985.

[6] H. Stubing and H.-M. Rein, IEEE Trans. Electron Dev., vol. 34, no. 8, pp. 1741-1751, Aug. 1987.

[7] H. Jeong and J. G. Fossum, IEEE Trans. Electron Dev., vol. 34, no. 1, pp. 124-131, Jan. 1989.

[8] H. K. Dirks, private communication.

[9] H. C. de Graaff and F. M. Klaassen, "Compact Transistor Modeling for Circuit Design," Springer-Verlag, 1990.

[10] P. B. Weil and L. P. McNamee, IEEE Trans. Circuits and Systems, vol. 25, no. 2, pp. 114-116, Feb. 1978.

[11] C. C. McAndrew and L. W. Nagel, pp. 144-147, Proc. 1994 BCTM.

[12] C. C. McAndrew, B. K. Bhattacharyya, and O. Wing, IEEE Trans. CAD, vol. 12, no. 6, pp. 825-828, Jun. 1993.

[13] W. J. Kloosterman and H. C. de Graaff, pp. 103-106, Proc. 1988 BCTM.

[14] C. Jacoboni, C. Canali, G. Ottaviani, and A. Alberigi Quaranta, Solid-St. Electron., vol. 20, pp. 77-89, 1977.

[15] J. A. Seitchik, C. F. Machala, and P. Yang, pp. 275-278, Proc 1989 BCTM.